

# MetaTracts - A Method for Robust Extraction and Visualization of Carbon Fiber Bundles in Fiber Reinforced Composites

Arindam Bhattacharya\*

The Ohio State University

Christoph Heinzl†

University of Applied Sciences - Upper Austria

Rephael Wenger‡

The Ohio State University

## ABSTRACT

This work introduces MetaTracts, a novel method for extracting and visualizing individual fiber bundles as well as their weaving pattern in endless carbon fiber reinforced polymer (CFRP) materials, scanned by X-ray computed tomography (XCT).

For the purpose of characterizing larger areas of CFRP materials such as complete unit cells integrating the recurring weaving pattern, the proposed workflow is designed to handle XCT scans of low resolution, in which the individual fibers of the bundles to be extracted are not or just barely visible. The proposed workflow applies and extends methods originally presented for the field of diffusion tensor imaging in order to cope with the low data quality: First, a coarse version of integral curves is used to trace subsections of the individual fiber bundles in the woven CFRP materials. We call these sections MetaTracts. In the second step these extracted fiber bundle sections (MetaTracts) are clustered using a two step approach, wherein the first step clusters according to orientation and the second step clusters by proximity of the MetaTracts. Finally, the tool can also generate volumetric representations as well as surface models of the extracted fiber bundles to be exported for further analysis.

We evaluate the proposed workflow on a number of real world datasets and demonstrate that MetaTracts effectively and robustly identifies and separates different fiber bundles.

**Index Terms:** K.6.1 [Management of Computing and Information Systems]: Project and People Management—Life Cycle; K.7.m [The Computing Profession]: Miscellaneous—Ethics

## 1 INTRODUCTION AND MOTIVATION

Modern industry is increasingly demanding function orientation, integration, and efficiency of novel materials and future components. The material of choice of a strongly growing number of applications are carbon fiber reinforced polymers (CFRP), which allow an integration of those continuously rising demands in industry. CFRPs have been successfully introduced in aeronautic and automotive applications within recent years, replacing more and more parts made of conventional materials such as aluminum or steel. But besides the aerospace and automotive industry, CFRP is also being used in a wide range of applications such as marine and civil engineering, automotive and wind turbine design, and also sporting goods manufacturing.

In general, CFRP materials show highly desired characteristics as high specific stiffness, high specific strength, high corrosion resistance at considerably lower weight compared to conventional materials. At the same time highly complex and integrated components may be produced from CFRPs, which were previously impossible to manufacture. For example even primary structures

and highly loaded components in aeronautics are been increasingly manufactured from CFRP.

Typically, carbon fiber reinforced polymer components, more specifically CFRP laminates consists of two main components:

The matrix on the one side, which acts as a bonding component and the reinforcements on the other side, which allows for achieving the desired characteristics. To manufacture CFRP laminates with endless carbon fibers, various production processes are in industrial use. Most of these processes start with the reinforcement component by weaving individual carbon fiber bundles (yarn) into sheets of carbon fiber cloth in a predefined pattern. These sheets of woven carbon fiber cloth, which form the geometrical structure of the final CFRP materials, are also referred to as fabric. Depending on the requirements of the final component as well as on the manufacturing process, fabrics may be stacked in multiple layers of the cloth. Both alignment of fabrics and the weaving pattern of the individual carbon fiber bundles strongly influence the strength, durability and stiffness properties. Next, resins are integrated in the material system to fill the gaps in the fabric, forming the matrix component. The main function of this matrix component is to act as a bonding component between the individual carbon fiber bundles. For the matrix of CFRP material systems with endless carbon fibers typically resins such as epoxy are frequently used. In special applications additional filler materials, such as colors or other particles, may be integrated.

The increasing share of CFRPs and also the complexity of both material system as well as the final components generated a strong demand towards non-destructive testing (NDT) techniques for quality control [20]. Ultrasonic testing is yet the most commonly used method for non-destructive testing of carbon fiber reinforce polymers. On the one hand ultrasonic testing provides a quick and cost-efficient overview. But on the other hand it shows low resolution and may generate arbitrary results, e.g. due to the geometry of the final component.

Aside ultrasonic testing, industrial 3D X-Ray computed tomography (XCT, also referred to as 3DXCT or cone beam XCT) is increasingly applied for non-destructive testing of fiber reinforced polymers [15]. XCT generates a 3D volumetric representation of the scanned specimen, reconstructed from a series of 2D penetration images, which taken throughout a full rotation of the specimen. In industrial XCT, the typical scanning geometry foresees the specimen to be placed on the rotary table between X-ray source and detector. X-rays are emitted by the source in the form of a conic beam. When passing through the specimen the X-rays get attenuated by the material in the specimen. The detector records the corresponding 2D attenuation image (penetration image), depending on its principle e.g. by transferring the X-rays in a scintillator layer into visible light. To generate the required series of 2D penetration images of a full 360° rotation for a complete reconstruction of the data volume, the specimen is rotated stepwise and at each position a cone beam penetration image is recorded [12]. Finally the series of penetration images is finally reconstructed to a 3D volumetric dataset of the specimen. In state of the art devices, XCT can reach voxel sizes below 500nm. XCT generates high resolution volume data for comprehensive and detailed analyses of the test specimens. Unfortunately, there is still a trade-off between view-

\*e-mail: arindamb86@gmail.com

†e-mail: christoph.heinzl@fh-wels.at

‡e-mail:wenger@cse.ohio-state.edu

port and image resolution in XCT using cone beam geometry. The magnification reached within an XCT scan is determined by the specified distances between source and specimen as well as source and detector. The magnification therefore directly influences both resolution and viewport: higher resolutions decrease the viewport but showing more details while lower resolutions allow for larger viewports and thus larger portions of the specimen.

In this work we focus on datasets with larger viewports and lower resolutions where the single carbon fibers (filaments) are not or barely visible. Our domain experts are mainly interested in visualizing the geometric structures in the weaving pattern of fiber bundles in endless carbon fiber reinforced composites instead of high resolution studies of the individual fibers. Figure 1 provides an example of our targeted datasets. It also shows the recurring fiber bundle pattern in the final CFRP laminate, called a *unit cell*. Our work is motivated from the recent progress in two interrelated fields: On the one hand, CFRP components have gained wide application in a variety of industries because of its superior material and physical properties in comparison to conventional materials [14]. On the other hand, recent developments of industrial 3D X-Ray computed tomography (XCT) with regard to larger detectors, larger field of views and better resolutions opened XCT for this new application area of non destructive testing for fiber reinforced components [24].

While fiber bundles are now understood as highly important in determining component properties, the tools for visualization of the internal structure have not developed at the same pace. To the best of our knowledge, there is no current work that can resolve simple queries such as:

- How to extract and visualize the geometric structure of a particular fiber bundle?
- How to visualize the interaction between a particular pair of fiber bundles (crossovers/braiding) or a unit cell?
- Which fiber bundles show a particular orientation?
- Which fiber bundles are of the same type of yarn (i.e. which bundles show similar sizes or diameters), which is the largest or smallest fiber bundle?

Extracting the answer to the above queries from the volume renderings of XCT datasets, or from visual inspection of particular 2D slices is non-trivial even for experts. We detail and evaluate a method which uses visualization techniques to gain insight into our data. We demarcate the above queries into two parts, “geometric structure” and “spatial context”. Geometric structure refers to the shape, size, and orientation of a fiber bundle or a group of bundles. Spatial context refers to how two or more bundles interact with each other. We advance and interpret techniques from diffusion tensor imaging to extract and visualize geometric structures from 3D X-Ray computed tomography data of the woven carbon fiber reinforced composites. The main goal of this work is to expand the state of the art in non destructive testing through visualization of composite structures in “lower resolutions” and thus “larger areas” of woven fabrics.

The paper is structured as follows: Section 2 reviews the related work, Section 3 describes the characteristics of our data. Sections 4, 5, 6 provides details of our approach. Section 7 details experiments and Section 9 explains our parameter choices. We end with conclusions.

## 2 RELATED WORK

Diffusion Magnetic Resonance Imaging (dMRI, also referred to as Diffusion Tensor Imaging (DTI)) has gained popularity in medical diagnosis within recent years. Its main clinical application is found in the study and treatment of neurological disorders. DTI may reveal abnormalities in white matter fiber structure and allows

for visualizing the organization of white fibers in the human brain as well as the brain connectivity. A variety of algorithms have been proposed aiming to generate fiber-tract trajectories. In general, these reconstructions of fiber trajectories are then clustered in to bundles which are expected to be related anatomically or spatially. We broadly divide the related work on DTI into two parts which are of immediate relevance to our proposed solution: fiber tracking and fiber clustering. Furthermore methods analyzing the second order local structure are also discussed. Finally, we review the current state of the art in the visual analysis of fiber reinforced composites.

### 2.1 Fiber Tracking in Diffusion Tensor Imaging

In detecting fiber tracts as shown by Basser et al. [2], [1] and Mori et al. [18], [17], the key idea is based on the assumption that the principal eigenvector of the diffusion tensor is parallel to the underlying dominant fiber direction in each image voxel. In these techniques, continuous tracts are created by propagating a virtual particle from a starting point until they reach a termination criterion. This is usually done by solving a second-order Runge-Kutta integration. The assumption is that the principal diffusion direction at each discrete location can be interpolated to form a continuous velocity field. One of the short comings of the process is that because of the local decision-making process, these methods perform poorly in noisy regions and often generate small fibers. Basser et al. [2], [1] proposed that white matter tracts could be represented as 3D curves in space. They showed that numerical methods could be used to follow fibers and fiber bundles and to generate tracts in human brain data. Mori et al. [18] showed that tract reconstruction techniques could be broadly divided into line-propagation or energy minimization techniques. In line propagation approaches, trajectories are computed based on local neighborhoods. While, energy minimization approaches find the most favorable trajectory connecting two given endpoints.

### 2.2 Fiber Clustering in Diffusion Tensor Imaging

The general assumption of fiber clustering in diffusion tensor imaging is that a similarity measure based on factors such as proximity between fibers can be used to interpret a collection of fiber tracts as bundles. Extensive research has been done on automatic DTI fiber clustering methods

The clustering approach divides the problem into two parts. The first part deals with finding a suitable proximity measure and the second deals with the choice of the clustering method. Pairwise proximity measures include, endpoint distances [6] and mean of the closest distances between points on two fibers [7]. Zhang et al. [27] introduced a thresholded version of the of the above distance so that fibers that are close for certain distance and then diverge are clustered separately. Brun et al. [5] uses normalized cuts along with a pairwise distances measure computed using a 9-D fiber shape descriptors. The choice of the clustering algorithm can be broadly divided into those approaches using hierarchical clustering (see [16], [27]) and those using spectral clustering (see [13], [19], [5])

Brun et al. [6] described how a spectral non-linear dimensionality reduction technique, Laplacian eigenmaps proposed by Belkin and Niyogi [3] can be applied to the problem of organizing fiber trace data. The key notion of the Laplacian eigenmaps algorithm is to represent the underlying data as a graph. Each node represents a data point and the edges connect neighboring data points. An eigenvalue problem is solved to represent the data in a lower dimensional space while preserving the local graph structure. In the case of fiber bundles, the individual points are fiber traces. In the ideal case fiber traces which belong to the same bundle must remain “close” to each other in the lower dimensional space. Westin et al. [26] also uses spectral clustering on a Hausdorff distance measure defined as the maximum of pointwise minimum distances between two fibers.

Jonasson et al. [13] runs k-means clustering on the eigenvectors of the affinity matrix defined as the co-occurrence of fibers in the data.

The agglomerative hierarchical clustering method [8] has gained popularity for proximity based fiber segregation Zhang et al. [27], Corouge et al. [7]. These approaches build on the assumption that proximity measure that compare DTI fiber trajectories can also represent anatomical relationship. An agglomerative hierarchical clustering method starts with each data point/fiber in an individual cluster. At each stage of the algorithm the two most similar clusters are joined. The two basic cluster similarity measures are single-link and complete-link. With the single link measure the distance between the clusters is the distance between the closest pair of items. Mobergs et al. [16] implemented several distance measures in their evaluation of fiber clustering and concluded that clustering methods are generally accurate in capturing fiber bundles.

The difficulties in hierarchical clustering include: first, computing all pairs distances for tracts to generate the distance matrix (see [11] for a recent work on decreasing computation times). Second, choosing the “correct” distance measure to compare tracts. Thirdly, hierarchical clustering is best suited for similar length fibers. Spectral methods are also hindered by long matrix computations.

### 2.3 Second order local structure

Unlike DTI, we do not have diffusion tensor data. Instead, we have a scalar volume with tubular structures embedded in them. Analyzing curvilinear structures in volumetric images has been utilized for a variety of purposes including center line extraction [4] and vascular image enhancement as proposed by Frangi et al. [9] and Sato et al. [23]. Frangi et al. [9] introduced a method based on studying the eigenvalues of the local second order structure namely the Hessian matrix, specifically for the purposes of developing vessel enhancement filters.

### 2.4 Visual Analysis of Fiber Reinforced Composites

The approaches presented in visualization and analysis of composites mainly focus on individual objects such as fibers or pores: Fritz et al. [10] proposed interactive workflows for non destructive testing practitioners to explore and quantify steel fibers in reinforced sprayed concrete. This approach allows analyzing fiber orientations based on direction transfer functions. Salabberger et al. [22] introduced a pipeline to extract and characterize individual fibers of fiber reinforced composites. They encode the extracted fibers as color-coded line segments in 3D and visually identifying fibers with similar orientations. Reh et al. [21] introduced an approach to explore pores of carbon fiber reinforced composites. Recently, Weissenbock et al. [25] introduced a system for interactive exploration and analysis of fibers in fiber reinforced polymers.

Tools based on image analysis, fiber tracking and clustering into bundles in DTI and their subsequent visualization through stream tubes and coloring schemes has received extensive research and recently the application of similar techniques to fiber tracing in composite materials has gained momentum. To the best of our knowledge there is no approach focusing on direct extraction of fiber bundle structures from low resolution XCT of composite fibers, which is the main scope of this work.

## 3 DATA CHARACTERISTIC AND ASSUMPTIONS

Figure 1 shows dataset1 with woven fiber bundles. Dataset1 is 450x300x500 voxels in size with isotropic resolution of  $2\mu m$ , the datatype is uint8. It clearly shows the weaving structure of the composite unit cell as regional subset of the recurring fiber bundle weaving pattern. The unit cell is used as a basis structure for CFRP manufacturing. The alignment and weaving pattern of the fiber bundles in the cloth influences the strength and stiffness properties of the resulting material. Figure 1(A) shows a volume rendering of the

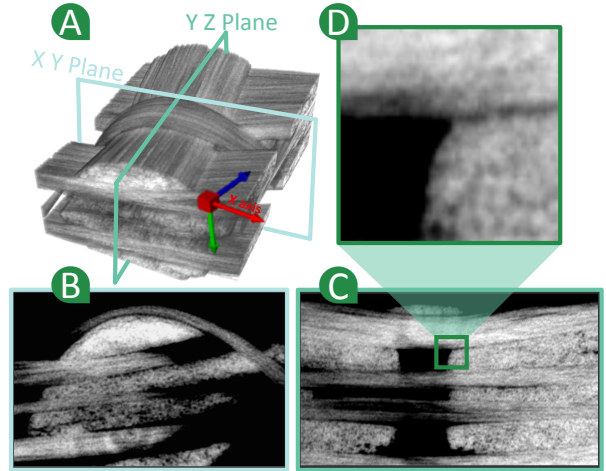


Figure 1: Data Characteristics. (A) shows a rendering of the data. (B) shows 2D slices along the X and (C) along the Z axis. (D) close up of the region marked in green in (C), multiple fiber bundles cross and are indistinguishable by visual inspection alone.

dataset. Fig. 1(B) shows 2D slices along the X and Fig. 1(C) in Z(left) axis. Figure 1(D) shows the zoomed in version of the green square. The resolution of dataset1 renders the individual carbon fibers in a fiber bundle are hard to resolve using 2D slice images only. Figure 1(D) contains two bundles going in opposite directions. However, the separation between two fiber bundles is barely visible. The carbon fibers themselves do not differ much from the underlying epoxy matrix in terms of attenuation which poses an additional challenge for characterization. The fiber bundles themselves may differ in terms of the amount of fibers in the bundle, figure 1(A) shows the large variation in cross section sizes among the bundles. Depending on the weaving pattern the fiber bundles cross each other in different orientations. In general the number of orientations is limited by the weaving pattern. In all our data sets the number of separate orientations was two. Nevertheless, the weaving pattern may cause the individual bundles to be curved. In consequence of the weaving pattern of the fiber bundles, individual fibers may be adjacent in euclidean distance but belong to different bundles. We make the following assumptions on our data:

- The structure embedded in the data contains fiber bundles of indiscernible fibers.
- (Local orientation) Each point within a fiber bundle has a local orientation which is parallel to the corresponding area in the fiber bundle.
- The local orientation may change gradually inside the fiber bundle.
- The local orientation may be noisy and not reliable.
- (Connectivity) Moving along the direction of a non-noisy local orientation in small increments, we will reach another neighborhood with similar local orientation.
- Fiber bundles going in different directions only interact near the surface of contact.

## 4 EXTRACTING METATRACTS

Figure 2 shows our pipeline. The approach consists of multiple steps. MetaTracts generations Sec. 4 and finding plausible fiber bundles (Section 5).

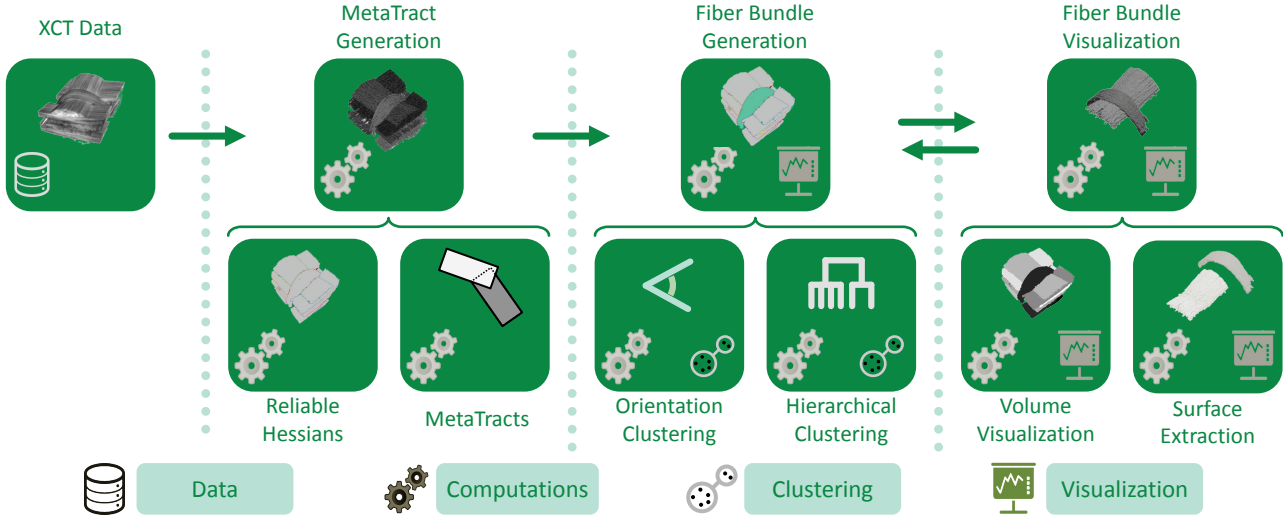


Figure 2: Flow chart of the MetaTracts approach for fiber bundle extraction

#### 4.1 Reliable Hessians

The input to the first stage of our pipeline, is the original scalar dataset in a uniform lattice grid in  $\mathbb{R}^3$ . As output, each grid location becomes associated with a vector representing the local orientation and a real value [0,1] which represents a measure of the reliability of the local orientation. We approximate the local orientation by eigenvalue analysis of the Hessian matrix computed at each voxel. The principal directions, in which the local second order structure of the image can be decomposed are given by the eigen decomposition of the Hessian matrix which describes the local curvature. The eigenvector corresponding to the smallest eigenvalue gives the direction along which the curvature is smallest. This direction coincides with the direction of the tubular structure.

Frangi et al. [9] introduced a process that searches for geometric structures which are tubular. They define a measure based on two geometric ratios of the second order ellipsoid given by the local Hessian matrix to measure the “vesselness” criterion. In order to determine reliable Hessians, we compute a similar metric. We include their work here for completeness and direct the reader to [9] for details. Let  $\lambda_K$  be the eigenvalue with the  $K^{th}$  smallest magnitude. Here  $|\lambda_1| \leq |\lambda_2| \leq |\lambda_3|$  are the eigen values of the Hessian matrix. Specifically, a pixel belonging to a vessel region will have small  $\lambda_1$  ( $|\lambda_1| \approx 0$ ) and  $\lambda_2, \lambda_3$  of large magnitude and of equal sign ( $|\lambda_1| \ll |\lambda_2|$  and  $|\lambda_2| \approx |\lambda_3|$ ). The sign indicates if the vessel is bright in a dark background or dark in a bright background. In our case the individual fibers are bright ( $\lambda_2, \lambda_3 < 0$ ). The following measures are defined in their work [9].

$$\mathcal{R}_{\mathcal{A}} = \frac{\text{Largest Cross Section}/\pi}{\text{Largest Axis Semi-length}^2} = \frac{|\lambda_2|}{|\lambda_3|} \quad (1)$$

$$\mathcal{R}_{\mathcal{B}} = \frac{\text{Volume}/(4\pi/3)}{(\text{Largest Cross Section Area}/\pi)^{\frac{3}{2}}} = \frac{|\lambda_1|}{\sqrt{|\lambda_2\lambda_3|}} \quad (2)$$

In equation 2,  $\mathcal{R}_{\mathcal{B}}$  provides a measure of deviation from a blob like structure while in equation 1,  $\mathcal{R}_{\mathcal{A}}$  distinguishes between plate-like and line-like structure. Grey-scale variations and close proximity of the fibers in our data make the Hessians computed at each voxels susceptible to errors. Thus we compute a measure, “equal” to the “vesselness” measure to determine which locations in the volume

provide reliable local orientation.

$$R_H = \begin{cases} 0 & \text{if } \lambda_2 > 0 \text{ or } \lambda_3 > 0 \\ (1 - e^{-\frac{|\lambda_{\mathcal{A}}|^2}{2s^2}})(e^{-\frac{|\lambda_{\mathcal{B}}|^2}{2s^2}})(1 - e^{-\frac{s^2}{2c^2}}) & \text{otherwise} \end{cases}$$

Variable  $s$  is the Frobenius norm of the Hessian matrix. The value of  $(1 - e^{-\frac{|\lambda_{\mathcal{A}}|^2}{2s^2}})$  will be low in regions with no structure. The utility of the vesselness is a little different in our framework than Frangi et al. [9]. First, in biology vesselness is computed for different scales because the vessels can be of different sizes. In our case, usually the width of individual fibers are known a priori. Second, and more importantly, we do not have clear tubular structures embedded in a dark contrast matrix such as in blood vessels. Instead, we are trying to associate each grid location with a probable orientation based on its local second order structure. The  $R_H$  is interpreted as a reliability measure of the local orientation. Grid locations where the  $R_H$  is above a certain threshold are marked as regions with reliable orientations. We use 0.3 as the cutoff for all our test cases. (See Section 9 on the choice of 0.3). In Figure 3 we see the intermediate results of the local orientation computation only at locations where  $R_H$  is greater than the cutoff threshold. The unit vector representing the principal direction has been mapped to RGB color space. Figure 3A shows the entire data set. Regions where the principal direction is parallel to the X axis are red in color, directions parallel to Y are green and those parallel to the Z are blue. Figure 3B and C show 2D slices along the Z and X axis respectively. Figure 3D shows a close up (region similar to Figure 1D). Note, the dark regions within a bundles are regions where the  $R_H$  is less than the threshold. The bundles are not uniformly colored, the Hessians and the corresponding directions are noisy.

We note some intrinsic differences between the DTI and our XCT data. Fiber traces can be created in DTI using a standard fiber tracking algorithm following the principal direction of diffusion using a fourth order Runge-Kutta method [6]. The principal direction based on the Hessian matrix works best when the tubular structures are well separated from the surrounding, this is not the case for our data. The local orientation at each voxel is inherently more noisy. Thus techniques popular in DTI cannot be directly applied in XCT data.

#### 4.2 MetaTracts properties and description

The input to this step is a grid in  $\mathbb{R}^3$  where each grid point is associated with a normalized local orientation and a corresponding  $R_H$

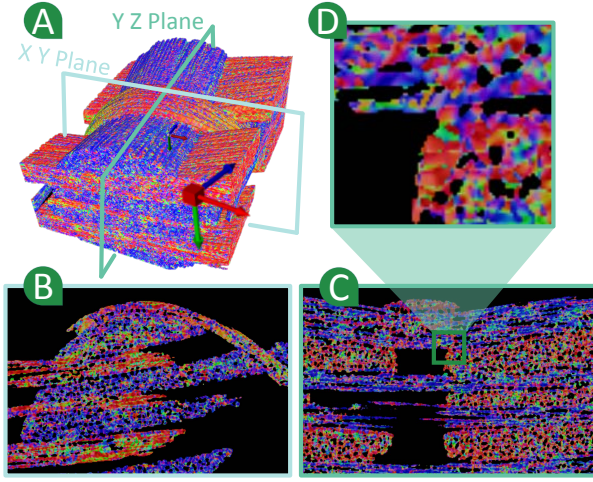


Figure 3: Reliable Hessians. (A) Colored according to Orientation vector mapped to RGB. (B) 2D slice along Z and (C) along X axis. (D) close up of the region marked in green in C.

value. Traditional integral curve based techniques cannot be used to extract fiber bundle traces from the reliable Hessians because of the spurious nature of the Hessian based local orientation. Thus instead of building fiber traces, we wish to find an abstract representation of the fibers. We build on the key assumptions on the data, namely ‘local orientation’ and ‘connectivity’ while taking into account the noise and lack of resolution. We do this by interpreting the underlying geometric structure of the fibers as a set of polylines (cylinders). MetaTracts are a coarse and simple approximation of integral curves in the form of a continuous chain of cylindrical tubes in  $\mathbb{R}^3$  traversing the fiber bundles embedded in the input data. MetaTracts share the following *properties*:

1. Each MetaTract is associated with a continuous set of cylinders.
2. Each MetaTract is associated with a start point which is a grid vertex.
3. Each cylinder in a MetaTract has a constant length, a constant radius and a start point (which is also a grid vertex).
4. Each cylinder in a MetaTract (except for the first one) is connected to the previous cylinder at its start point.
5. Each cylinder is locally parallel to the local orientation at its start point.

### 4.3 MetaTracts generation

In  $\mathbb{R}^2$  all the above properties hold except that cylinders are replaced by rectangles. We explain the process of MetaTracts generation in  $\mathbb{R}^2$ . The procedure trivially extends to  $\mathbb{R}^3$ . The reliable Hessian step generates a local orientation in  $\mathbb{R}^2$  and a  $R_H[0,1]$ . In Figure 4 all regions which have reliable Hessian less than the threshold have been marked in blue. Let the seed point associated with the MetaTract be grid point  $C_p$  (Property 2, Section 4.2). The local orientation at  $C_p$  as computed in the step above is  $N_p$  and is given by the dark green arrow (Figure 4C). We generate a rectangle of length  $L$  and radius  $R$ , the green dashed rectangle shows the rectangle generated at  $C_p$  (Property 3 and 5, Section 4.2). The set of vertices which are in the green region but not overlapped by blue are possible candidates for the start point of the next cylinder in a particular MetaTract. We call these vertices “*candidate vertices*”.

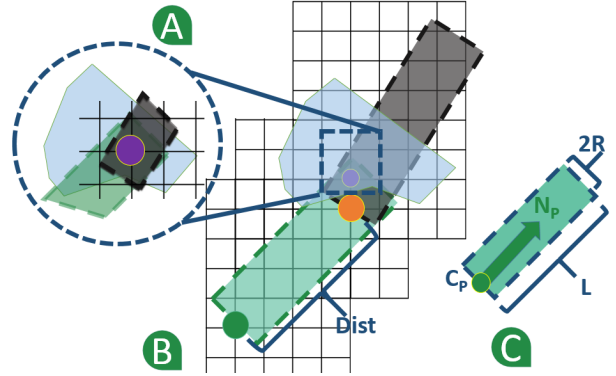


Figure 4: MetaTracts generation: (B) MetaTract generation, region with  $R_H$  less than threshold. (A) close up of marked region in (B). (C) Parts of a single MetaTract.

From these we select another grid vertex which will be the start point for the next cylinder. The order of the candidate vertices is based on the following characteristics:

- *Orientation Similarity*: We want the orientation of the start points for the consecutive cylinders to have a similar orientations ( $N_p$ ).
- *Large distance*: We want the MetaTracts to traverse the data using as few cylinders as possible. Thus, we want the distance between  $C_p$  and the start point for the next cylinder to be as large as possible. We measure distance of a grid vertex from  $C_p$  by projecting the Euclidean distance between them onto  $N_p$ . For example the Euclidean distance between the blue and the orange vertices projected onto  $N_p$  gives distance (Figure 4B). We refer to this perpendicular projection distance as “dist”.

We further define a priority for each of the candidate vertices based on the above factors. For each cylinder in a MetaTract, we put the *candidate vertices* of it in a priority queue based on Equation 3.

$$\text{Priority} = \gamma_1 e^{(-\text{angle}^2/\alpha^2)} + \gamma_2 e^{(-\text{dist}^2/\beta^2)} \quad (3)$$

$\gamma_1, \gamma_2$  are the weights ( $\mathbb{R}_{\geq 0}$ ) which decide how the priority depends on the affine combination of the two factors. For all our cases we use ( $\gamma_1 = 1/3$  and  $\gamma_2 = 2/3$ ). In general we suggest  $\gamma_1 + \gamma_2 = 1$  and  $\gamma_1 \leq \gamma_2$ . At each iteration we pick the top element in the priority queue generate the corresponding cylinder and repeat the steps. Essentially, Equation 3, selects a grid point which is the furthest from the current point and going in a similar direction. This gives it the advantage of tackling noise/errors in local orientation better than integral curves by looking at multiple choices for vertices and avoiding intra cell interpolation (for orientation) in an already noisy environment.

In this particular example in Figure 4(B) we select the orange grid vertex next and repeat the process. We do not select the purple vertex (Figure 4(C)) because it is not a candidate vertex. If we generate tracts that have erroneous local orientations they will not be able to find further possible candidate vertices and will be of short length. Short tracts are then removed. The MetaTracts generated are shown in Figure 5A. The MetaTracts are colored with the mean orientation direction mapped to the RGB space. That consistent orientation is a key intrinsic feature in the data becomes visually pronounced. We apply uniform, dense seeding to the XCT volume data to trace and generate the tracts of fiber bundles.

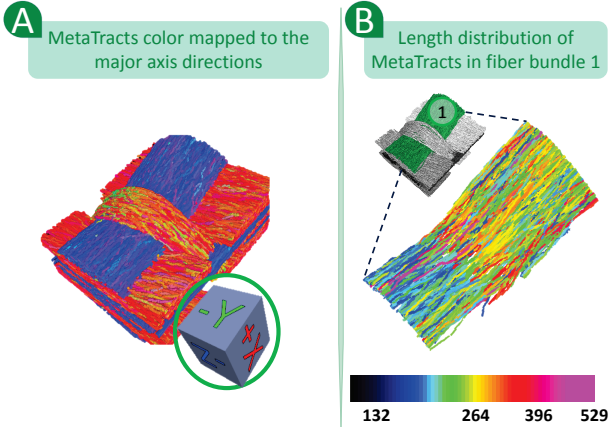


Figure 5: (A) MetaTracts colored according to mean orientations. (B) length distribution of individual MetaTracts for a particular bundle.(unit for length is grid cube edge length)

## 5 FIBER BUNDLE GENERATION

The output of the above step is a set of MetaTracts. In this step we focus on clustering the MetaTracts into plausible bundles. We use hierarchical clustering which has enjoyed considerable attention and success in DTI field. However, often the MetaTracts produced in Section 4 do not extend the full length of the fiber bundle. Thus, MetaTracts in a given fiber bundle may have very different lengths and may only partially overlap as in Figure 5B. Moreover, carbon fibers have both orientation and proximity information which can be used for clustering. Instead of creating an heuristic, which artificially combines the two measures, we first cluster based on orientation and then further subdivide each orientation cluster using proximity information. We found that different clustering methods were preferable for the different measures. We use dimension reduction followed by K-means clustering for orientation clustering while we use hierarchical clustering to further subdivide each cluster based on proximity measures (see Section 7 for experimental results). Breaking clustering into two steps also helps us and potential users to better understand the results of the clustering.

### 5.1 Orientation based clustering

This step divides the individual MetaTracts into classes based on their major orientations. In order to cluster MetaTracts going in same directions, we use a spectral embedding technique called Laplacian eigenmaps which was originally introduced by Belkin and Niyogi [3] and later used in DTI fiber coloring [6] and fiber clustering [5]. The key notion is to find a suitable similarity measure to define the weights of an undirected weighted graph. The nodes being the data points and the edges being the weights. Then, an eigenvalue problem is solved, which maps the manifold embedded in the graph into a lower dimensional space while preserving the graph structure. This lower dimensional space can then be clustered more efficiently than the higher dimensional space. Let  $G$  be the graph, we compute the eigenvalues and eigenvectors for the generalized eigenvector problem:  $L\mathbf{f} = \lambda D\mathbf{f}$ , where  $D$  is the diagonal weight matrix and  $L$  is the Laplacian matrix. The eigenvector  $f_0$  corresponding to the eigenvalue 0 is left out and the next  $m$ ,  $f_1$  through  $f_m$  eigenvectors are used to embed in an  $m$ -dimensional space. K-means clustering is then used to cluster in this lower dimensional space.

Brun et al. [6] based their measure on the simple assumption that two traces with similar endpoints should be considered similar. Brun et al. [5] based their measure on a 9-D fiber descriptors. In our case, each MetaTract is a data point. We introduce a simple

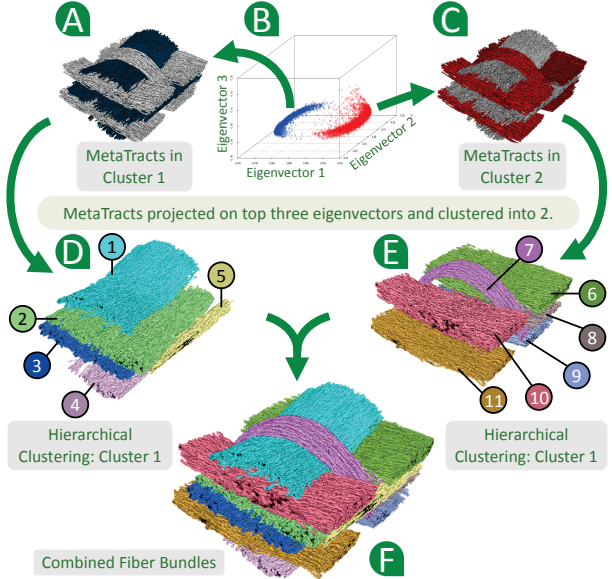


Figure 6: (B) Result of K means clustering with data points projected to the top three eigenvectors as major axes. (A) MetaTracts belonging to orientation cluster 1. (C) MetaTracts belonging to orientation cluster 2. MetaTracts in gray(A,C) show context. (D,E) shows the result of distance based clustering on the orientation cluster. (F) shows the combined result.

*orientation based similarity measure.* There is no spatial information involved, just a partition of the MetaTracts based on orientation which is already inherent in the data. Following this, given a pair of MetaTracts, we define the edge weights between two tracts as the cosine of the maximum angle between the local orientations ( $N_P$ ) of all pairs of start points ( $C_P$ ) between the two MetaTracts. The edge weights give a distance matrix representing the distance between each pair of points. Using the Belkin and Niyogi algorithm we “embed” these points in a low dimensional space where the Euclidean distance between points approximates the distance between points given by the distance matrix. We used conventional K-means for clustering this lower dimensional space. Here  $K$  is supplied by domain knowledge of the number of major fiber bundle directions of the woven structure. For our test case there are two major directions of the fiber bundles. So  $K$  was set to 2. It is important to note that due to the advantages offered by the dimensionality reduction, even if there are curved fibers bundles the user has to provide just the major fiber bundle directions of the weaving pattern. Figure 6B shows the result of the K-means clustering with the data points projected to the top three eigenvectors as the major axes. As is expected there is a clear distinction based on fiber orientation. Figure 6(A,C) shows the MetaTracts colored according to clustering results.

### 5.2 Distance based clustering

Orientation clustering uses only orientation information. To subdivide the oriented clusters into fiber bundles, we need to include further information about the geometric proximity between MetaTracts. We use the directed Hausdorff distance for distance based clustering. Each MetaTract is represented as a set of points ( $C_P$ ). Formally, the directed Hausdorff distance from point set  $P$  to point set  $Q$  is defined as  $H_{dir}(P, Q) = \max_{p \in P} \min_{q \in Q} d(p, q)$ . The Hausdorff distance is defined as  $H(P, Q) = \max(H_{dir}(P, Q), H_{dir}(Q, P))$ . The Hausdorff distance is a metric so  $H(P, Q) \leq H(P, Q') + H(Q', Q)$  but the directed Hausdorff is not. Unfortunately, the Hausdorff distance does not work well for our application since a fiber bundle may have many MetaTract which only partially

covers the bundle (Figure 5(B)). If a MetaTract  $P$  covers only part of the fiber bundle covered by  $Q$ , then  $H_{dir}(P, Q)$  will be very small while  $H_{dir}(Q, P)$  will be large. Thus,  $H(P, Q)$  will be large, even though  $P$  and  $Q$  are in the same fiber bundle. Instead of using the Hausdorff distance,  $\max(H_{dir}(P, Q), H_{dir}(Q, P))$ , we use  $\min(H_{dir}(P, Q), H_{dir}(Q, P))$ . If  $P$  covers only part of the fiber bundle covered by  $Q$ , then  $\min(H_{dir}(P, Q), H_{dir}(Q, P))$  is very small. Note that if  $P$  and  $Q$  overlap but do not cover the same parts of the fiber bundle, then  $H_{dir}(P, Q)$  and  $H_{dir}(Q, P)$  and  $\min(H_{dir}(P, Q), H_{dir}(Q, P))$  will be large.

The directed Hausdorff distance is very sensitive to outliers in the data. However, because MetaTracts after orientation clustering are constructed using cylinders with similar orientations, they are not plagued by outliers. To cluster based on MetaTract proximity, we used single linkage hierarchical clustering. Hierarchical clustering has a single parameter  $h$ , the desired number of clusters. In hierarchical clustering each objects starts in its own cluster and clusters are merged based on some criterion. Clusters are merged until there are only  $h$  clusters left. Hierarchical clustering is intuitive since it is easy to trace how clusters are formed and merged. Single linkage clustering finds pairs of objects  $p \in P$  and  $q \in Q$  where  $P \neq Q$  which are closer than other such pairs, and merges the containing clusters  $P$  and  $Q$ . We found that single linkage hierarchical clustering had two major drawbacks. First, the clustering would produce some small clusters of just a few MetaTracts. These MetaTracts were anomalies caused by noise in the data and did not represent true fiber bundles. Second, if two fiber bundles were parallel for some of their length and then separated, they would sometimes be clustered into the same fiber bundle. A short MetaTract which was parallel to both and did not extend into the separation region could form a link between the two fiber bundles, causing them to be clustered into a single bundle. To address the problem of small clusters, we applied hierarchical clustering and then identified small clusters with few MetaTracts. We removed the MetaTracts that were in those clusters from the data set and reapplied hierarchical clustering. To address the problem of short MetaTracts joining different fiber bundles, we applied hierarchical clustering and then removed the shortest fibers (fibers less than 0.6 times the median length) in each bundle. We then reapplied hierarchical clustering. We repeated both until a steady state of clusters is reached and no new small fibers can be removed. The results of clustering the orientation clusters Fig. 6(A,C) are shown in Fig. 6(D,E) respectively. Note how the purple cluster Fig. 6(E) bundle “7” is extracted well.

## 6 VOXELIZATION AND SURFACE EXTRACTION

Apart from direct visualization of the MetaTracts, we show two simple yet highly important extensions for our domain specialist. The first one is to voxelize the original volume according to the clusters each voxel is associated with. The second is to extract the corresponding surfaces from the voxel data by binarizing the volume per cluster and extracting the isosurface of the largest connected component from the binary volume. Both methods can possibly be used for further analysis of the data, e.g. in simulations. To voxelize the space, we compute a neighborhood around each voxel. We then enumerate the number of voxels of each class (cluster) in this neighborhood. The voxel is then assigned to the class with the maximum number of elements in the neighborhood. Figure 7A and Figure 8D shows the result of voxelization. Figure 7(C, D) show examples of extracted meshes.

## 7 EXPERIMENTAL RESULTS

We tested our method on multiple datasets with varying characteristics. Figure 6 shows the result of data set 1 decomposed into 2 orientation and each orientation decomposed into 10 clusters (the ground truth is 6 and 5 respectively). The hierarchical clustering is robust to over segmentation. Figure 9 shows the median, minimum

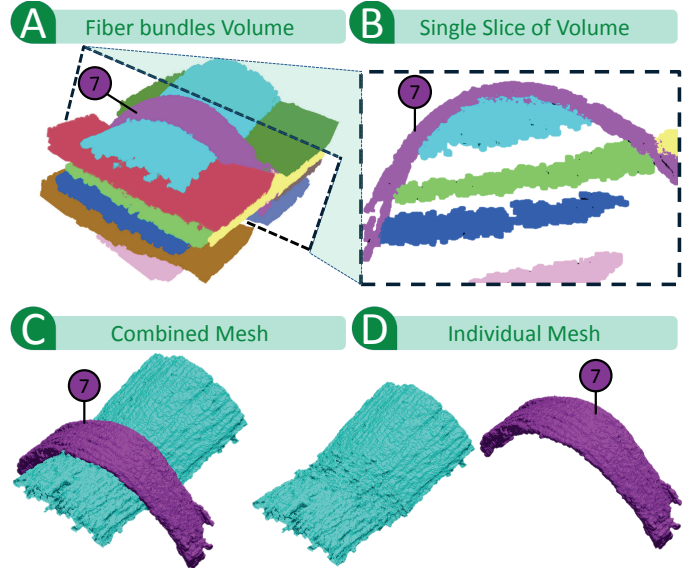


Figure 7: (A) Volume rendering of data set Figure 1A.(B) shows a single slice of the data set. (C) shows two of the extracted meshes together. (D) shows the meshes separately.

Figure 8: Data set with flat thin and compact bundles. (A) shows the volume rendering and a 2D slice with one of the boundaries marked in green, (B) shows the clusters according to individual orientation. (C) shows the complete result. (D) shows the voxelization of (C).

and maximum lengths per cluster. We generate the correct clusters and outlier bundles with very few elements which can be discarded. As noted in section 5.2 the tracts do not run the entire length of the dataset, the median length of MetaTracts in cluster 6 Fig. 5 is 200 while the maximum MetaTract in the bundle is about 500 (measured in units of grid cube length). Fig. 5(B) shows the length per MetaTract distribution for a particular fiber bundle. Fig. 8 shows the results on our dataset2. This dataset is dense with flat and thin bundles. The dimensions are 300x350x300 and the datatype is uint16 (compared to dataset1 which was only uint8). The bundles are indistinguishable in the original data set Fig. 8(A). A green dotted line shows one of the fiber bundle boundary. Fig. 8(B) shows the fiber bundles for the two orientation. Fig. 8(C) shows the combined results. Fig. 8(D) shows the volume after voxelization. The fiber bundle extraction using MetaTracts was implemented in C++ using ITK. All clustering was done in R. The preprocessing consists of MetaTract generation the distance computation and the orientation clustering. The hierarchical clustering separately, on the results of the orientation clusters can be done quickly in a few minutes on a Intel Xeon E5-2667 workstation according to user input ‘ $h$ ’(section 9). We store the normalized direction at each fiber point, thus both distance measures can be extracted simultaneously without extra computation.

## 8 USER EVALUATION

We integrated MetaTracts into a tool and created a user evaluation questionnaire which we distributed.

## 9 PARAMETER CHOICES

The critical parameters are  $K$  for the K-means in orientation based clustering and  $h$  for the hierarchical clustering.  $K$  denotes the number of major directions, which is either known a priori or can be easily estimated by looking at the weaving pattern. Our framework

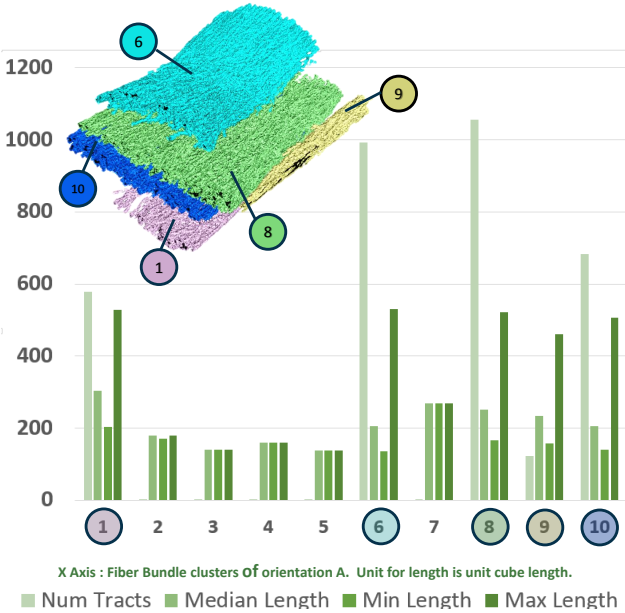


Figure 9: Number of tracts and median, minimum and maximum length of individual MetaTracts in the orientation cluster Fig. 6, clustered into 10 clusters (Fig. 7A top). The unit for length is the grid cube length. Figure 5(B) shows the length of individual MetaTracts in cluster 6. Clusters labeled 2,3,4,5 and 7 all have cardinality less than 10.

is robust to the choice of  $h$  (Section 7). Large  $h$  keeps the major bundles intact. For example, in Fig. 9, where  $h$  was set to ten while the ground truth was five, we observe that the major clusters remain well segmented and small clusters can be removed if they have too few elements (clusters 2,3,4,5 and 7 in Fig. 9 all have less than 10 elements). This is an appealing trait of the proximity based clustering, thus providing good results even when exact  $h$  might be unknown. The following parameters were fixed for all the tests. We set the reliable Hessian threshold  $R_h$  to be 0.3 for all our tests. A  $R_h$  of 0.0 would mean all points have reliable local orientation which would cause spurious MetaTracts detection. On the other hand a very high  $R_h$  would lead to be a decline in number of MetaTracts produced. The  $\alpha$  and  $\beta$  in  $R_h$  are as explained in Frangi et al. [9] and set to 0.5. The length and the width parameters for the cylinders for the MetaTracts decide how coarse the fiber cylinders are. Larger cylinders will handle noisy local orientation better as it inspects a higher number of candidate points to extend the fiber. We used 10.00 and 2.00 for length and breadth, respectively for all tests.  $\alpha$  and  $\beta$  in equation 3 decide how quickly the value of the factor decays, we have used [7-10] and half the length of cylinder (5.0). Our number of fiber bundle directions are limited, thus even for small  $\eta$ , the distinction between the orientation clusters is preserved quite well. We compared  $\eta = 3 - 7$  experimentally without any dramatic change in results.

## 10 CONCLUSION AND FUTURE WORK

In this paper, we introduce a framework to extract and visualize fiber bundles in composite materials. We show that our framework works at comparatively low resolution and with dense fiber arrangements (when extracting single fibers might not be possible). It handles complex fiber patterns such as “cross overs” and “braiding”. The presented techniques are attractive and novel features for a industrial fiber bundle visualization tool.

## REFERENCES

- [1] P. J. Basser, S. Pajevic, C. Pierpaoli, and A. Aldroubi. Fiber tract following in the human brain using dt-mri data. *IEICE TRANSACTIONS on Information and Systems*, 85(1):15–21, 2002.
- [2] P. J. Basser, S. Pajevic, C. Pierpaoli, J. Duda, and A. Aldroubi. In vivo fiber tractography using dt-mri data. *Magnetic Resonance in Medicine*, 44(4):625–632, 2000.
- [3] M. Belkin and P. Niyogi. Laplacian eigenmaps and spectral techniques for embedding and clustering. In *Advances in Neural Information Processing Systems 14*, pages 585–591. MIT Press, 2001.
- [4] S. Bouix, K. Siddiqi, and A. Tannenbaum. Flux driven automatic centerline extraction. *Medical Image Analysis*, 9(3):209 – 221, 2005.
- [5] A. Brun, H. Knutsson, H.-J. Park, M. E. Shenton, and C.-F. Westin. Clustering fiber traces using normalized cuts. *Lecture Notes in Computer Science*, 3216/2004(3216):368–375, 2004.
- [6] A. Brun, H.-J. Park, H. Knutsson, and C.-F. Westin. Coloring of dt-mri fiber traces using laplacian eigenmaps. In *Computer Aided Systems Theory - EUROCAST 2003*, volume 2809 of *Lecture Notes in Computer Science*, pages 518–529. Springer Verlag, 2003.
- [7] I. Corouge, S. Gouttard, and G. Gerig. Towards a shape model of white matter fiber bundles using diffusion tensor mri. In *Biomedical Imaging: Nano to Macro, 2004. IEEE International Symposium on*, pages 344–347 Vol. 1, April 2004.
- [8] R. O. Duda, P. E. Hart, and D. G. Stork. *Pattern Classification*. Wiley Interscience, 2 edition, 2000.
- [9] A. Frangi, W. Niessen, K. Vincken, and M. Viergever. Multiscale vessel enhancement filtering. In W. Wells, A. Colchester, and S. Delp, editors, *Medical Image Computing and Computer-Assisted Intervention MICCAI98*, volume 1496 of *Lecture Notes in Computer Science*, pages 130–137. Springer Berlin Heidelberg, 1998.
- [10] L. Fritz, M. Hadwiger, G. Geier, G. Pittino, and M. E. Gröller. A visual approach to efficient analysis and quantification of ductile iron and reinforced sprayed concrete. *IEEE Transactions on Visualization and Computer Graphics*, 15(6):1343–1350, 2009.
- [11] E. Garyfallidis, M. Brett, M. M. Correia, G. B. Williams, and I. Nimmo-Smith. Quickbundles, a method for tractography simplification. *Frontiers in neuroscience*, 6, 2012.
- [12] C. Heinzl. *Analysis and Visualization of Industrial CT Data*. PhD thesis, Institute of Computer Graphics and Algorithms, Vienna University of Technology, Favoritenstrasse 9-11/186, A-1040 Vienna, Austria, 12 2009.
- [13] L. Jonasson, P. Hagmann, J. Thiran, and V. Wedeen. Fiber tracts of high angular resolution diffusion mri are easily segmented with spectral clustering. In *International Society for Magnetic Resonance in Medicine*, volume 24, pages 1127–1137, 2005.
- [14] Y. Karpat, O. Bahtiyar, and B. Deer. Mechanistic force modeling for milling of unidirectional carbon fiber reinforced polymer laminates. *International Journal of Machine Tools and Manufacture*, 56(0):79 – 93, 2012.
- [15] J. Kastner, editor. *4th Conference on Industrial Computed Tomography*, Wels, Austria, September 2012. Shaker Verlag, Aachen.
- [16] B. Mobergs, A. Vilanova, and J. J. van Wijk. Evaluation of fiber clustering methods for diffusion tensor imaging. In *Visualization, 2005. VIS 05. IEEE*, pages 65–72. IEEE, 2005.
- [17] S. Mori, B. J. Crain, V. P. Chacko, and P. C. Van Zijl. Three-dimensional tracking of axonal projections in the brain by magnetic resonance imaging. *Annals of Neurology*, 45(2):265–269, 1999.
- [18] S. Mori and P. C. M. van Zijl. Fiber tracking: principles and strategies a technical review. *NMR in Biomedicine*, 15(7-8):468–480, 2002.
- [19] L. O’Donnell and C. F. Westin. Automatic tractography segmentation using a high-dimensional white matter atlas. *Medical Imaging, IEEE Transactions on*, 26(11):1562–1575, Nov 2007.
- [20] C. Red. Aviation outlook: Composites in general aviation 2011-2020. *High-Performance Composites*, May 2012.
- [21] A. Reh, B. Plank, J. Kastner, M. E. Gröller, and C. Heinzl. Porosity maps - interactive exploration and visual analysis of porosity in carbon fiber reinforced polymers. *Computer Graphics Forum*, 31(3):1185–1194, June 2012.
- [22] D. Salaberger, K. Kannappan, J. Kastner, J. and Reussner, and

- T. Auinger. Evaluation of computed tomography data from fibre reinforced polymers to determine fibre length distribution. In *International Polymer Processing*, volume 3, pages 283–291, 2011.
- [23] Y. Sato, S. Nakajima, H. Atsumi, T. Koller, G. Gerig, S. Yoshida, and R. Kikinis. 3d multi-scale line filter for segmentation and visualization of curvilinear structures in medical images. In J. Troccaz, E. Grimson, and R. Mosges, editors, *CVRMed-MRCAS'97*, volume 1205 of *Lecture Notes in Computer Science*, pages 213–222. Springer Berlin Heidelberg, 1997.
  - [24] P. J. Schilling, B. R. Karedla, A. K. Tatiparthi, M. A. Verges, and P. D. Herrington. X-ray computed microtomography of internal damage in fiber reinforced polymer matrix composites. *Composites Science and Technology*, 65(14):2071 – 2078, 2005.
  - [25] J. Weissenbock, A. Amirkhanov, W. Li, A. Reh, A. Amirkhanov, E. Groller, J. Kastner, and C. Heinzl. Fiberscout: An interactive tool for exploring and analyzing fiber reinforced polymers. In *Pacific Visualization Symposium (PacificVis), 2014 IEEE*, pages 153–160, March 2014.
  - [26] C.-F. Westin, S. E. Maier, H. Mamata, A. Nabavi, F. A. Jolesz, and R. Kikinis. Processing and visualization of diffusion tensor MRI. *Medical Image Analysis*, 6(2):93–108, 2002.
  - [27] S. Zhang, S. Correia, and D. H. Laidlaw. Identifying white-matter fiber bundles in DTI data using an automated proximity-based fiber-clustering method. *IEEE transactions on visualization and computer graphics*, 14(5):1044–53, 2008.